doi:10.1016/j.jmb.2005.02.039 J. Mol. Biol. (2005) 348, 183–193

JMB

Available online at www.sciencedirect.com

SCIENCE DIRECT®

ELSEVIER

Crystal Structures of Proto-oncogene Kinase Pim1: A Target of Aberrant Somatic Hypermutations in Diffuse Large Cell Lymphoma

Abhinav Kumar, Valsan Mandiyan, Yoshihisa Suzuki, Chao Zhang Julie Rice, James Tsai, Dean R. Artis, Prabha Ibrahim and Ryan Bremer*

Plexxikon, Inc., 91 Bolivar Drive Berkeley, CA 94710, USA

Pim1, a serine/threonine kinase, is involved in several biological functions including cell survival, proliferation, and differentiation. While *pim1* has been shown to be involved in several hematopoietic cancers, it was also recently identified as a target of aberrant somatic hypermutation in diffuse large cell lymphoma (DLCL), the most common form of non-Hodgkin's lymphoma. The crystal structures of Pim1 in apo form and bound with AMPPNP have been solved and several unique features of Pim1 were identified, including the presence of an extra β-hairpin in the N-terminal lobe and an unusual conformation of the hinge connecting the two lobes of the enzyme. While the apo Pim1 structure is nearly identical with that reported recently, the structure of AMPPNP bound to Pim1 is significantly different. Pim1 is unique among protein kinases due to the presence of a proline residue at position 123 that precludes the formation of the canonical second hydrogen bond between the hinge backbone and the adenine moiety of ATP. One crystal structure reported here shows that changing P123 to methionine, a common residue that offers the backbone hydrogen bond to ATP, does not restore the ATP binding pocket of Pim1 to that of a typical kinase. These unique structural features in Pim1 result in novel binding modes of AMP and a known kinase inhibitor scaffold, as shown by co-crystallography. In addition, the kinase activities of five Pim1 mutants identified in DLCL patients have been determined. In each case, the observed effects on kinase activity are consistent with the predicted consequences of the mutation on the Pim1 structure. Finally, 70 co-crystal structures of low molecular mass, low-affinity compounds with Pim1 have been solved in order to identify novel chemical classes as potential Pim1 inhibitors. Based on the structural information, opportunities for optimization of one specific example are discussed.

Keywords: Pim1; kinase; crystal structure; somatic hypermutation; scaffold discovery

**Corresponding author*

Introduction

pim1 is a proto-oncogene originally identified as a preferential proviral integration site in Moloney murine leukemia virus-induced T-cell lymphomas.[1] Pim1 is the first described member of a unique family of serine/threonine kinases, which includes at least two other kinases (Pim2 and Pim3) with significant sequence homology to Pim1.[2,3] Several substrates of Pim1 phosphorylation have been identified, including c-Myb,[4] BAD,[5,6] SOCS-1,[7] Cdc25A,[8] HP1,[9] PAP-1,[10] $p21^{cip1/waf1}$,[11] PTP-U2S,[12] and NFATc1.[13] Pim1 has been shown to have diverse biological roles in cell survival, proliferation, and differentiation.[14] However, mice lacking all three *pim* genes have recently been shown to be viable and demonstrate that the PIM kinases are

Present address: V. Mandiyan, Department of Pharmacology, Yale University School of Medicine, 333 Cedar Street, New Haven, CT 06510, USA.

Abbreviations used: DLCL, diffuse large cell lymphoma; RMSD, root-mean-square deviation; PDB, Protein Data Bank.

E-mail address of the corresponding author: rbremer@plexxikon.com

important for growth factor signaling, but are not essential for development.[15]

Dysfunction of Pim1 has been implicated in the progression of multiple cancers, including several hematopoietic and prostate cancers. Although the exact mechanisms by which Pim1 participates in cell transformation have not been completely elucidated, several reports point to the ability of Pim1 to prolong cell survival.[16–18] Overexpression of Pim1 has been observed in myeloid and lymphoid acute leukemia and Pim1 is constitutively expressed in some myeloid leukemia cell lines.[19,20] Increased Pim1 expression has also been identified in neoplastic prostate cancer specimens from patients by cDNA microarray analysis and by anti-Pim1 antibody staining.[21] In a transgenic murine model of prostate cancer in which human c-*myc* is expressed, the gene expression profile is consistent with that seen in human prostate cancer, including upregulation of Pim1.[22] In addition, Pim1 may participate in deregulated cell growth in prostate cancer through the hormone-independent activation of the androgen receptor, a typical characteristic of advanced prostate cancer that offers poor patient prognosis.[23]

In diffuse large cell lymphoma (DLCL), the most common form of non-Hodgkin's lymphoma, *pim1* has been shown to undergo chromosomal translocations, resulting in its overexpression.[24] A recent study showed that *pim1* was also the target of an aberrant somatic hypermutation in DLCL.[25] Hypermutation sites are distributed in both the 5′ untranscribed region (UTR) and coding sequence, and independent of the chromosomal translocations. Notably, there are seven missense mutations introduced into the coding exons of the gene. These missense mutations may affect the three-dimensional structure and, in some cases, the kinase activity of the Pim1 protein. Hypermutations are also detected in *pim1* found in primary central nervous system lymphomas[26] and multiple subtypes of AIDS-induced non-Hodgkin's lymphomas.[27] Inhibition of Pim1 kinase activity by small molecules has the potential to offer a therapeutic benefit for treating these diseases.

We report here the crystal structure of Pim1 and the co-crystal structures of Pim1 in complex with small molecules, including an ATP analog, as well as determination of the relative enzymatic activities of Pim1 mutants found in DLCL and evaluation of effects of these mutations on protein structure. The apo Pim1 crystal structure is nearly identical with that recently reported while this work was in preparation.[28] However, differences are observed between the reported structure of AMPPNP bound to Pim1 obtained by soaking apo crystals with AMPPNP and the structure reported here obtained by co-crystallization.[28] Overall, these crystal structures reveal several unique features of Pim1 that distinguish it from other structurally characterized kinases. Most notably, Pim1 contains an insertion in the hinge region and a proline residue at a key position (position 123) critical for ATP binding. Other kinases have a non-proline residue at this position where the backbone NH of the residue makes a conserved hydrogen bond to ATP. We show, by X-ray crystallography, that changing P123 to methionine, a frequently occurring amino acid at this position in other kinases, does not restore the ATP binding pocket of Pim1 to that of a typical kinase, suggesting that the length of the hinge is an important determinant of the unique mode of adenine binding by Pim1. Another important difference between Pim1 and other kinases of known structure is the presence of a novel β-hairpin in the N-terminal lobe of the protein. Interestingly, the two turn residues of the hairpin are both subject to DLCL-associated somatic hyper-mutation.[25] We have measured the kinase activities of these and other missense mutations found in DLCL and identified mutations that significantly alter the enzymatic activity relative to wild-type Pim1. The observed kinase activities are consistent with the predicted effects of these mutations on the structure of Pim1.

We have also evaluated the binding of small molecules to the ATP site of Pim1. Due to the distinctive structural features of Pim1, unique binding modes were observed for AMP, as well as a known kinase inhibitor scaffold. The absence of a hydrogen bond donor in the hinge has a dramatic impact on the binding of these compounds, which alternatively exploit a conserved water-mediated hydrogen bond network in Pim1. For the purposes of novel inhibitor discovery, we have recently reported for another protein family the facile optimization of a low molecular mass, low-affinity compound selected based on the co-crystal structure complex.[29] In this approach, co-crystallography was applied early in the drug discovery process as a filter to screen low molecular mass, weakly active compounds for novel chemical scaffolds that interact with key features of the target protein and that subsequently can be developed into potent and selective leads guided by this structural information. In an analogous approach with Pim1, we have undertaken an extensive co-crystallography effort with small molecules, and solved over 70 different co-crystal structures of Pim1 with compounds representing various chemical scaffolds. Despite the chemical diversity of the compounds, several general features emerge as the most critical for compounds to satisfy the unusual binding requirements of Pim1. We report the common trends revealed by this ensemble of co-crystal structures, as well as one specific example and the opportunities to increase potency for this new scaffold based on the structural data.

Results

Overall structure

The crystal structures of Pim1 reported here are based on a construct containing only the catalytic

domain (residues 29–313)[30] of the protein. The 2.0 Å structure of human Pim1 apo enzyme determined here is essentially identical with the apo structure solved by Qian *et al*. (RCSB PDB code, 1XQZ),[28] using the full-length protein construct. The Pim1 catalytic domain adopts the characteristic bilobular kinase fold,[31] with a novel two-stranded β-sheet preceding the α_C helix that distinguishes it from all other kinases. The relative arrangement of the two lobes is similar to the closed, activated conformation of kinases first established by the structure of cyclic AMP-dependent kinase (cAPK; PDB code, 1ATP).[32] The structurally conserved ion pair of active kinases is present in Pim1 between K67 of β_3 and E89 of α_C. In all the Pim1 structures that have been determined, the activation loop adopts a conformation characteristic of the activated kinase state,[28,33] despite the absence of phosphorylated residues that is typically observed in other activated kinases. There is no conformational change in the activation loop between the apo Pim1 enzyme and any of the ligand-bound binary complexes described below. As noted by Qian *et al*., an elaborate network of hydrogen bonds and hydrophobic interactions play an important role in stabilizing the observed active conformation.

Comparing Pim1–AMPPNP complex structures

We co-crystallized Pim1 along with an ATP analog, AMPPNP, and determined the binary complex structure to 2.0 Å. Surprisingly, the complex structure obtained by co-crystallography is significantly different from that reported by Qian *et al*.,[28] who harvested their binary complex by soaking the apo-crystal with AMPPNP. The key difference between the two structures lies in the conformation of the G-loop (residues 46–54) (Figure 1). Qian *et al*. report that AMPPNP binding causes a dramatic change in the conformation of the G-loop. The backbone RMSD value between the binary and the apo-structures in this region is 4.6 Å, and the C^{α} of F49 was displaced by up to 7 Å. In contrast, the G-loop backbone conformational change in our complex structure is relatively modest (2 Å RMSD). Although residue F49 swayed away from the ATP binding site, to leave room for the γ-phosphate group of AMPPNP, the side-chain of F49 remained largely buried in our structure. In contrast, the F49 in 1XR1 appears to dock into a hydrophobic cleft created by a neighboring molecule in the crystal lattice and is partially solvent-exposed.

Additionally, the γ-phosphate group makes unusually close contacts with the active site residues of the enzyme in our Pim1–AMPPNP binary complex structure. The distance between the γ-phosphate oxygen atom (O2G) and the carboxylate oxygen atom (OD2) of D186 is only 1.6 Å. The same γ-phosphate oxygen atom is positioned 2.1 Å from the side-chain oxygen atom (OD1) of N172. These distances suggest that the current structure may mimic a meta-stable intermediate state of the enzyme–ATP substrate complex.

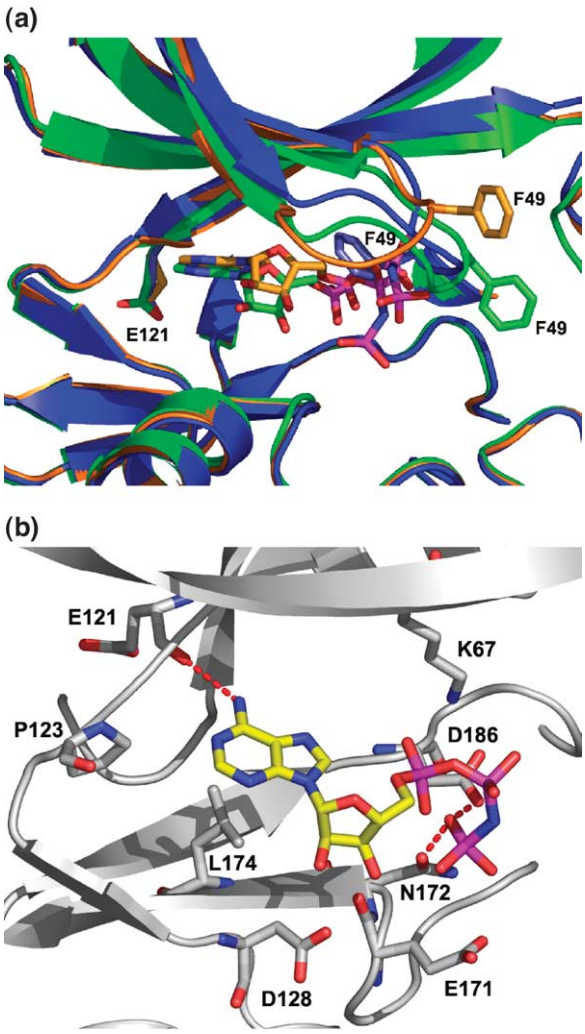

Figure 1. Comparison of Pim1–AMPPNP complex structures. (a) Overlay of the active site region of Pim1 as observed in our structures (apo-blue; AMP–PNP complex green) and the AMPPNP complex reported by Qian *et al.* (orange).[28] The Figure highlights the differences in conformations of both AMPPNP and the G-loop between the two structures in reference to the apo structure. (b) AMPPNP bound to Pim1. The close contacts between the γ-phosphate group of AMPPNP and D186 and N172 are indicated by a broken red line. The hydrogen bond between the E121 carbonyl oxygen atom and N6 of AMPPNP is also indicated with a red broken line. This and all subsequent Figures were generated using Pymol http://pymol.sourceforge.net.[46]

The hinge

The Pim1–AMPPNP complex structure shows a unique feature that distinguishes Pim1 from all other kinases of known structure. The difference lies in the hinge region where, in addition to the hydrogen bond between the N6 atom of adenine and the backbone carbonyl oxygen atom of the first

hinge residue (corresponding to residue 121 of Pim1), other kinases also form a second conserved hydrogen bond between the N1 atom of adenine and the backbone NH of the third hinge residue (corresponding to residue 123 of Pim1). In fact, this hydrogen bond donor and acceptor pair is regarded as one of the structural signatures of the kinase family. Unlike other kinases, residue 123 in Pim1 is proline, which is incapable of making a hydrogen bond with the ATP due to its lack of the amide hydrogen. Additionally, a structure-based alignment of Pim1 with other structurally characterized kinases (Figure 2(a)) shows that the hinge of Pim1 is at least one residue longer than those of other kinases. This insertion causes the region to bulge out from the ATP binding pocket (Figure 2(b)). As a result, the distance between the backbone nitrogen atom of P123 and N1 of the adenine is 4.8 Å, significantly longer than the range allowed for a hydrogen bond.

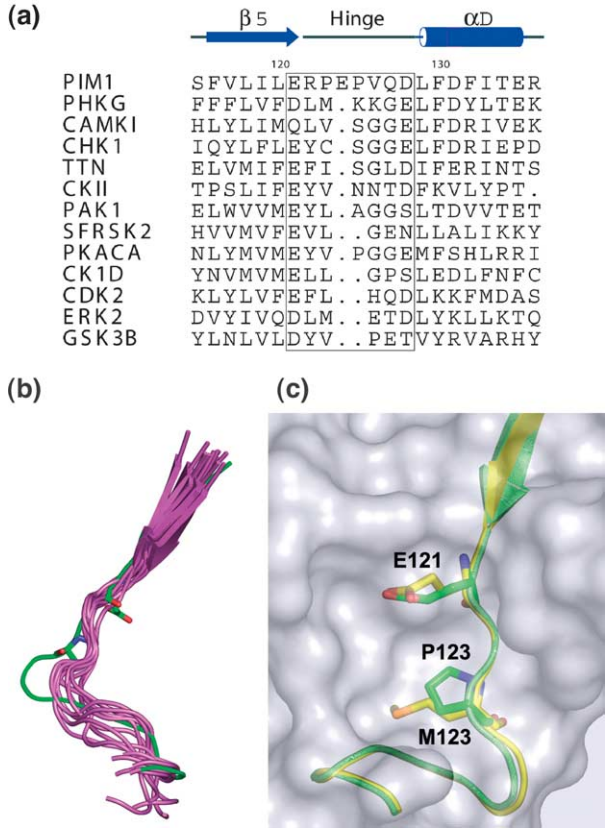

Figure 2. Hinge structure. (a) A sequence alignment of the hinge region of selected Ser/Thr kinases indicates the presence of the proline residue at position 123 in Pim1 and an insertion of an extra residue following P123. The secondary structure elements, beta strand β_5 and the helix α_D, flanking the hinge region (boxed) are labeled at the top. The proteins used in the alignment are PHKG, CAMKI, CHEK1, TTN, CKII, PAK1, SFRSK2, PKACA, CK1D, CDK2, ERK2, and GSK3B. (b) A structural alignment of the hinge region of the selected kinases in (a) shows the position of the residues E121 and P123 of Pim1 (green) and a bulge in the hinge caused by the presence of an extra residue compared with other kinases. (c) An alignment of the hinge region between Pim1 wild-type protein (green) and the mutant P123M (yellow) reveals an absence of any conformational change between the two structures. A surface rendition of the Pim1 shows a small depression in the surface of the wild-type protein that is sealed by the side-chain in the P123M protein.

We investigated whether a mutation of P123 to a non-proline residue can provide the amide hydrogen for hydrogen bonding to ATP as in other kinases. Specifically, the residue P123 was mutated to methionine, and the structure of the mutant was determined at 2.1 Å resolution. The conformation of the hinge backbone is nearly identical between the mutant and wild-type protein (Figure 2(c)). Consistent with the structural data, the P123M mutant demonstrated similar kinase activity to the wild-type in the biochemical assay (Figure 3(b)). Although the attempt to co-crystallize the P123M mutant protein with ATP or an ATP analogue was not successful, an examination of co-crystal complexes of the P123M mutant with four other small molecules (data not shown) revealed no conformational change in the mutant structures *vis-à-vis* the wild-type protein, suggesting that it is unlikely that a bound ATP molecule is able to induce a large conformational change required to bring the backbone NH of M123 within hydrogen bonding distance to ATP.

The nearly identical structures of the hinge in the wild-type Pim1 and the mutant enzyme underscore the importance of contributions made by other residues in the hinge region in stabilizing the observed conformation. A further experiment showed that a deletion of residue E124 in combination with P123M caused the protein to lose kinase activity completely (Figure 3(b)) and to fail to crystallize despite extensive trials. The adverse effect caused by shortening the hinge suggests that the atypical length of the hinge is important for Pim1.

DLCL-associated mutations in Pim1

Pasqualucci *et al.*[25] reported seven missense mutations in *pim1* identified from tumor DNAs in human DLCL cases. Of the seven mutations, five were identified in exons 3 and 4, which code for the catalytic domain of the protein (Figure 3(a)). In order to understand the effects of these clinical mutations, we cloned all five mutants and measured their kinase activity in an *in vitro* biochemical assay. One mutant (H68Y) showed a substantial increase in the activity of the enzyme compared to the wild-type, while three mutants (P81S, N82K and L193F) displayed a decreased kinase activity, and one mutant (E135K) demonstrated no significant difference in activity (Figure 3(b)).

Because the Pim1 structure reported here represents the active conformation of the kinase, we hypothesize that an activating mutation stabilizes this conformation, whereas an inactivating mutation disrupts the conformation. In the Pim1 structure H68 is surrounded by hydrophobic

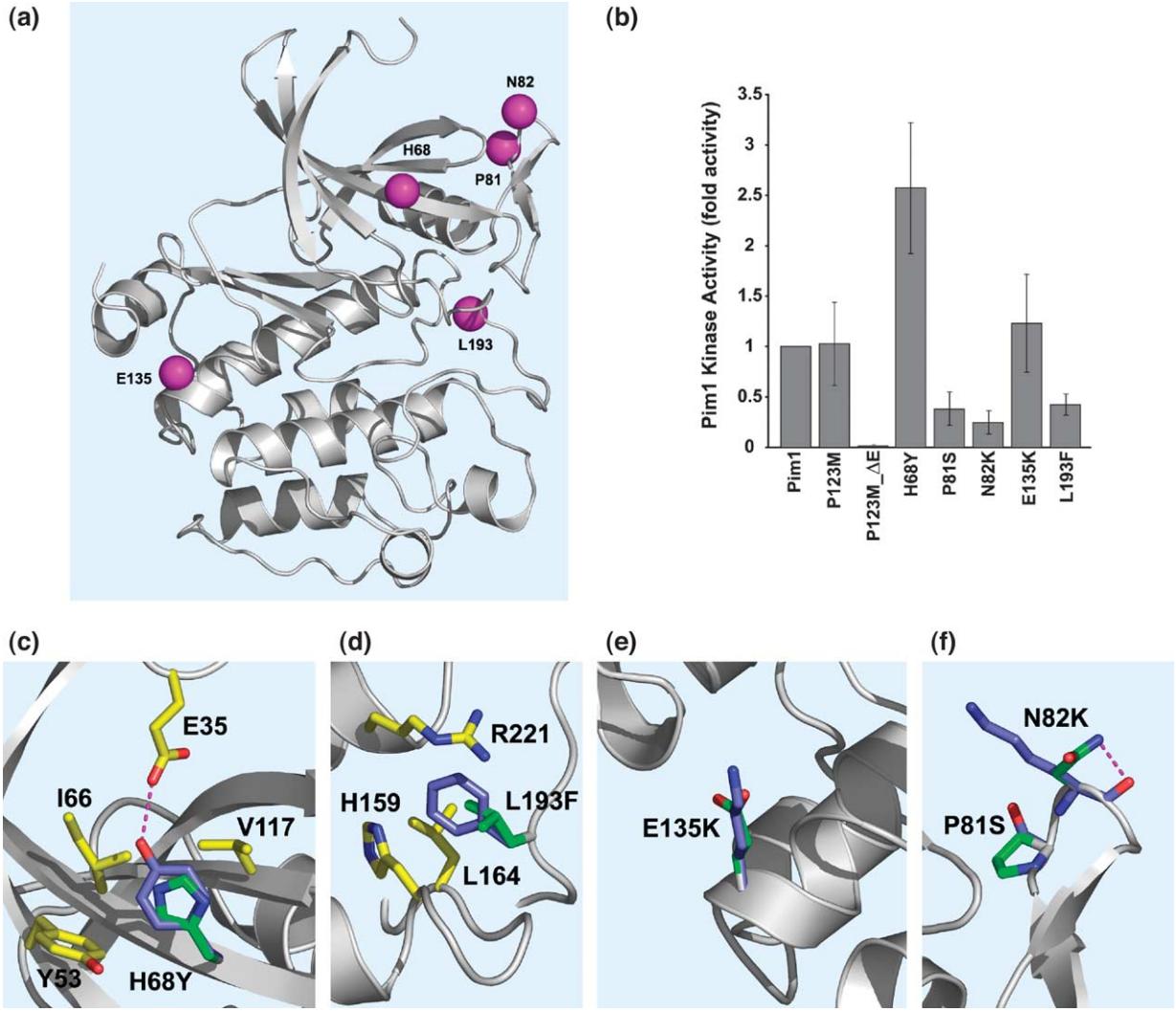

Figure 3. The mutational data. (a) Locations of the clinically observed point mutations in DLCL have been indicated on the protein structure. (b) A histogram shows the *in vitro* kinase activity, relative to wild-type Pim1, of these mutants, as well as that of P123M and P123M_ΔE. Error bars are the standard deviations of three experiments. (c)–(f) The side-chain conformations of these residues (green) with the modeled mutations (blue). Surrounding residues affected by these mutations are depicted in yellow.

side-chains from three residues Y53, I66, and V117 (Figure 3(c)). The phenol group of a tyrosine residue substituted at this position fills this hydrophobic pocket more completely, and its hydroxyl group can form an additional hydrogen bond with E35. Therefore, the H68Y mutation is expected to promote the active state of the kinase, consistent with the 2.5-fold increase in activity observed for the Pim1-H68Y mutant. On the other hand, the activation loop mutation L193F is likely to be a destabilizing mutation because L193 packs very well into the surrounding residues in the structure (Figure 3(d)) and changing it to phenylalanine would disrupt the existing packing. The additional bulk of the phenylalanine would make it more difficult for the activation loop to adopt the activated conformation. Consequently, Pim1-L193F was found to be nearly 2.5-fold less active than wild-type. Interestingly, the mutant Pim1-E135K showed no noticeable change in kinase activity. Because E135 is exposed to solvent, no significant structural change is expected by replacing glutamate with lysine (Figure 3(e)).

Mutations of two residues in the β-hairpin preceding the regulatory α_c-helix, P81 and N82, were found to severely impair the kinase activity. Both proline and asparagine are pro-turn residues. Substitution of the proline at residue 81 with serine resulted in a mutant with 2.6-fold less activity than wild-type Pim1 (Figure 3(f)). Furthermore, the Pim1 structure revealed an interesting pattern of intra-residue interaction, with the N82 side-chain ND2 atom hydrogen bonded to its backbone CO (Figure 3(f)). A substitution of N82 to lysine, therefore, will preclude this interaction and is expected to destabilize the β-turn motif. The Pim1-N82K mutant was found to be fourfold less active than wild-type. The sensitivity of kinase activity to the

features of this β-hairpin preceding the α_c helix further suggests that this unique feature of Pim1 may be important in regulating the kinase.

Binding modes of AMP and a known kinase inhibitor scaffold

Crystal structures of known kinase inhibitors bound to the ATP pockets of different kinases show that almost all inhibitors bind to the backbone of the third hinge residue (residue 123 in Pim1 numbering), and most inhibitors also bind to the first residue of the hinge, the same hydrogen bonding pattern used in ATP binding.[34] Given the unique hinge conformation of Pim1 and the lack of a hydrogen bond donor at position 123, it is of significant interest to examine how Pim1 binds small molecule ligands.

One of the most dramatic examples of an unusual ligand-binding mode is provided by the Pim1–AMP co-crystal structure. The crystallographic asymmetric unit contains four protein–ligand complexes with AMP binding in two distinct binding modes, both of which are significantly different from the binding of the AMP group in the AMP–PNP structure (Figure 4). In the first binding mode (Figure 4(a)), AMP surprisingly flips 180° from the AMP–PNP conformation shown in Figure 1, and as a result, the ribose group now sits inside the pocket and the 3′OH joins an extensive hydrogen bond network formed inside the pocket by K67, E89, the backbone NH of F187, and a water molecule (W1). This hydrogen bond network is a key structural signature in Pim1 that is observed in many co-crystal structures where W1 is highly conserved (*vide infra*). In the second binding mode (Figure 4(b)), the N6 atom of AMP points towards K67 and E89, whereas the 3′OH group of AMP now interacts with the carbonyl oxygen atom of Glu121, the canonical hydrogen bond acceptor of the hinge described previously. Because the exocyclic amine of AMP can only act as a hydrogen bond donor, it cannot substitute OH in its capacity to serve both as a hydrogen bond donor and as acceptor. This may explain why the second binding mode is observed in only one subunit, whereas the first binding mode is observed in three of the four subunits.

Another example of the consequences of the lack of a hydrogen bond acceptor in the Pim1 hinge on small molecule binding can be observed in the co-crystal structure with a compound (PLX-K031) containing a known kinase inhibitor scaffold, oxindole. Oxindoles have previously been co-crystallized with FGFR1[35] and CDK2.[36] In both cases, the oxindole scaffold makes the two canonical hydrogen bonds to the protein backbone of the hinge, between the N1 atom of the oxindole and the carbonyl oxygen atom of the first hinge residue (E562 of FGFR1 and E81 of CDK2), and between O2 of the oxindole and the amide nitrogen atom of the third hinge residue (A564 of FGFR1 and L83 of CDK2). The orientation of the oxindole of PLX-K031 in Pim1 (Figure 4(c)) is almost opposite from that of the scaffold in FGFR1 or CDK2. Neither N1 nor O2 of the oxindole core forms a hydrogen bond with the hinge backbone. Instead, the phenol attached to the oxindole is found deep inside the pocket, with its terminal hydroxyl group participating in

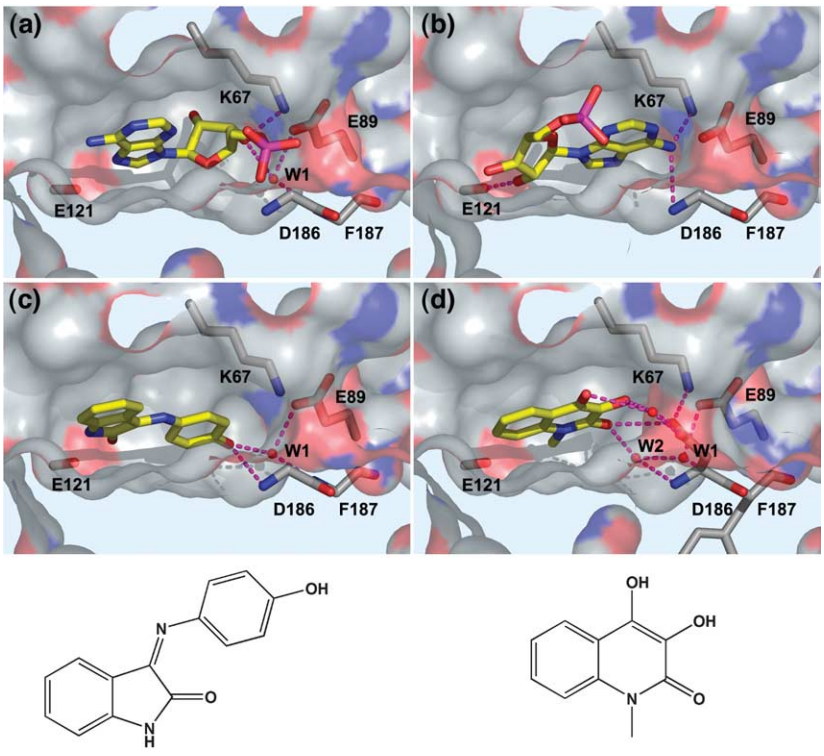

Figure 4. Small molecules binding in the ATP binding pocket of Pim1. The small molecules are shown in stick representation bound to the protein in the ATP binding site. The hinge region in each of these figures is located on the left side and a few residues have been labeled. Water molecules are denoted by red spheres. The carbon atoms on the protein surface are colored white, and the electronegative and electropositive atoms are colored red and blue, respectively. (a) and (b) The two binding modes of AMP in Pim1. (c) PLX-K031 and (d) PLX-K063 show small molecules bound to the protein, highlighting the role of structural water molecules in ligand binding to Pim1. The chemical drawing of these compounds are depicted below each panel.

the conserved water (W1) mediated hydrogen bond network near K67 and E89 in a direction similar to the 3′OH of AMP. This result supports the notion that the canonical hydrogen bond donor from the hinge plays a critical role in anchoring known kinase scaffolds in their standard conformation. A lack of this structural element, as seen in Pim1, produces a protein with significantly altered selectivity towards small molecules.

Novel inhibitor scaffold discovery by co-crystallography

We have recently demonstrated success in using co-crystallography of a target protein with weakly inhibitory, low molecular mass, scaffold-like molecules as a means for the discovery of novel chemical classes that can be optimized for potency and selectivity.[29] In an analogous approach with Pim1, over 200 low molecular mass compounds

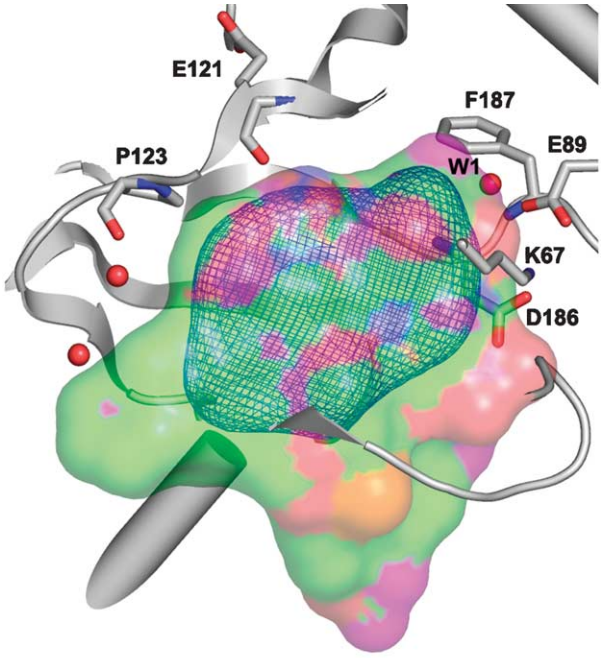

Figure 5. Overlay of the co-crystal structures of Pim1 with 70 different ligands. For clarity, only one representative structure of Pim1 and the molecular surface of the ligand ensemble are shown (the molecular surface is colored by atom types: red, oxygen; blue, nitrogen; green, carbon; sulfur, yellow; halogens, magenta). The blue mesh encloses a region where a large number of compounds overlap. The mesh represents a pseudo-electron density calculated using the ligand ensemble and is contoured at 1σ level above the mean, which roughly corresponds to 40 overlapping ligands. This is the region where the scaffold portion of a molecule is expected to bind. Three conserved water molecules that are observed in a majority of the 70 co-crystal structures are also shown (red spheres). Water molecule 1 (W1) plays a critical role in mediating a hydrogen bond network formed between many compounds and the interior of the ATP-binding pocket. The two other water molecules next to P123 help to define the boundary of the pocket.

(<350 Da) with weak inhibitory activity (>30% inhibition of Pim1 kinase activity at 200 μM compound concentration) in a biochemical assay were identified. After a high-throughput crystallography campaign, over 150 crystallographic data sets were collected and their structures determined. Of these, we observed compounds bound in the ATP binding pocket of the protein in over 70 instances (Figure 5). The high success rate of these weak inhibitors bound in Pim1 offers a rich pool of scaffold candidates and accompanying structural information for further evaluation. Optimization of such novel starting points has been shown to be a facile mechanism for efficiently obtaining bioactive compounds of much higher potency, while retaining favorable pharmacological properties.[29]

While a complete report of 70 co-crystal structures is beyond the scope of this work, some general trends can be clearly observed from an analysis of the binding site and the overlaps of the ensemble of inhibitor scaffold candidates. As shown in Figure 5, the inhibitor binding occurs exclusively in the ATP binding site of Pim1, with the majority of ligands localized near the hinge and the conserved K67/E89/F187/W1 hydrogen bond network. The dramatic effect of P123 on the ensemble of scaffold candidates can be easily identified. Not surprisingly, the atoms in closest proximity to P123 in the hinge are hydrophobic in nature (Figure 5, green atoms), rather than hydrogen bond accepting as is found in the conventional "donor–acceptor" interaction employed routinely in kinase–inhibitor complexes. In this regard, the ensemble provides many scaffold candidates that complement the unique nature of Pim1 and offer attractive starting points for design of a selective inhibitor. Of the small group of inhibitors that present oxygen-containing moieties in this region, many contain a nitro group as the presenting functionality, and thus represent an unconventional partner in this context, at best. The W1 hydrogen bond network is a key element in many Pim1 complexes with scaffold candidates. W1 is highly conserved and appears in more than 90% of the co-crystal structures.

An example of one particular scaffold candidate bound to Pim1 is shown in Figure 4(d). In this structure, PLX-K063 (3,4-dihydroxy-1-methyl-quinolin-2-one, 191 Da) is bound in the ATP binding site with multiple hydrogen bonding and hydrophobic interactions. The compound is situated between the hydrophobic sandwich formed by L44, V52, and A65 from one side, and L174 and I185 from the opposite side. The 3-OH of PLX-K063 is directly hydrogen-bonded to D186 and the 4-OH group makes a water- mediated interaction to this residue. The 2-carbonyl group is the entry point for the compound into the conserved W1 hydrogen bonding network, albeit through another water molecule, W2, which links to W1 and the backbone amide of D186. The 2-carbonyl group also makes a water-mediated hydrogen bond to K67 deeper in the pocket. These initial structural data serve as a foundation to elaborate this quinolinone scaffold

into a more potent lead and opportunities exist to additionally substitute the scaffold to make further interactions with the protein. For example, the E121 backbone carbonyl is appropriately positioned to form a hydrogen bond with donors on either the lactam or phenyl rings of the scaffold. Substitution of the 3-hydroxy group could release the bound water and make direct contacts to K67 and E89, in addition to D186. Further substitution of the phenyl ring with hydrophobic substituents at positions 7 or 8 would more intimately contact the hydrophobic surface established by P123. Finally, the 5 and 6 positions of the scaffold are directed toward the bulk water solvent and offer the opportunity to substitute the compound to modulate the overall physicochemical properties. In general, the optimization of a particular scaffold can be guided by the space occupied by the total ensemble of 70 scaffold candidates bound in the co-crystal structures (Figure 5) and specific interactions made by these ligands can be replicated in the selected scaffold as a means to increase potency.

Discussion

The proto-oncogene kinase Pim1 was discovered 20 years ago and recently great strides have been made in understanding the biological role of this important kinase in cell survival and proliferation. The compelling evidence of Pim1 involvement in various cancers has made it a promising new drug target. Because of the low level of sequence homology between the Pim family of proteins and other members of the kinase family,[37] the three-dimensional structure of Pim1 is especially important for understanding the biological function of Pim1 and for the design of potent and selective Pim1 inhibitors as novel therapeutic agents. The Pim1 structures reported here revealed a number of interesting distinctions from the traditional kinase fold and provide a rationale for the effects of clinically observed mutations on Pim1 kinase activity. In addition, Pim1 has proven to be an excellent system for co-crystallography of weakly active, low molecular mass, small molecules at the early stage of drug discovery.

The recent identification of *pim1* as a target of somatic hyper-mutation in non-Hodgkin's lymphomas made it particularly interesting to consider the potential effects of these mutations on the structure and, consequently, the kinase activity of Pim1. For each mutant studied, the observed enzymatic activity was consistent with the predicted effects on the Pim1 structure. While Pim1 kinase activity was determined here using an *in vitro* assay, the effects of Pim1 mutations may be quite different in a cellular context and extend beyond simply the relative kinase activities. For example, in the case of B-Raf, mutants with decreased kinase activities were still found to effect ERK phosphorylation efficiently *in vivo* through transactivation of a closely related kinase, c-Raf.[38] Similarly, Pim1 mutants that did not exhibit increased kinase activity in the *in vitro* assay may still participate in promoting cell survival through altered interactions with other proteins. Each of the amino acid mutations studied here is on the surface of Pim1 and could potentially participate in protein–protein interactions. The β-hairpin preceding the α_c regulatory helix is unique to Pim1 and the kinase activity data suggest that it may play a role in modulating the enzyme. Notably, residues of the β-hairpin have been identified as points of hypermutation in other non-Hodgkin's lymphomas, in addition to DLCL.[26,27] Further experimental studies are required to elucidate the downstream effects of Pim1 hypermutations *in vivo*.

While a variety of kinase inhibitor classes have emerged in the last decade, the known kinase inhibitors that we have tested have little or a very weak effect on Pim1 (data not shown). This is not surprising given the absence of the canonical hydrogen bond donor in the hinge region that is a key element for binding of many kinase inhibitors and the altered backbone conformation caused by the longer hinge region in Pim1. This is also consistent with our observation of atypical binding modes for molecules such as AMP and an oxindole.

Low molecular mass compounds provide a rich, untapped source of novel scaffolds for drug discovery. Such molecules offer the opportunity to accommodate additional substitutions for optimization while retaining favorable pharmacological properties. This can be a particularly effective tactic when coupled with a structure-guided approach.[29] To identify the most promising candidates, it is beneficial to filter for a minimal inhibitory activity and use co-crystallography to evaluate the quality of compounds based on their interactions with key features of the protein and their potential for modification to increase potency and selectivity. Pim1 has proven particularly amenable to the initial steps of this approach with 70 co-crystal structures of compounds bound in the ATP binding site observed from 150 collected datasets. This ensemble of scaffold candidates reveals how diverse compounds can satisfy the unusual binding requirements of Pim1 and provides the foundation for optimization of a selected scaffold.

Materials and Methods

Cloning, expression, purification and crystallization of Pim1

The *pim1* cDNA fragment, encoding amino acid residues 29–313 (Gene accession no. NM_002648), was amplified from a human brain hippocampus cDNA library (Clontech, 7169-1) by PCR protocol and cloned into a pET29a vector (Invitrogen), in-frame with a carboxyl-terminal His_6 tag for bacterial expression. The protein was expressed in *Escherichia coli* cells with an overall yield of 20–25 mg/l. It was purified by cobalt affinity column, followed by size-exclusion and anion-exchange chromatography. The isolated protein was

characterized by N-terminal sequencing. All Pim1 mutants reported here were expressed and purified using the same protocols. To assist in solving the apo Pim1 crystal structure, a Pim1 derivative, selectively substituted with seleno-methionine (Se-Met), was also prepared, using known procedures.[39] The protein was crystallized by a sitting-drop, vapor-diffusion experiment in which equal volumes of protein (10–15 mg/ml concentration) and reservoir solution (0.4–0.9 M sodium acetate, 0.1 M imidazole (pH 6.5)) were mixed and allowed to equilibrate against the reservoir at 4 °C. This same condition also produced crystals for both the P123M mutant and protein co-crystal complexes. To obtain co-crystals of complexes of the protein with ligands, the protein solution was initially mixed with the compound (dissolved in dimethyl sulfoxide (DMSO)) at a final compound concentration of 1 mM, and then set up for crystallization using the method described above. The crystals routinely grew to a size of 200 μm×200 μm×800 μm in about two to three days. The crystals for the Se-Met protein were grown against a reservoir solution containing 0.1 M Tris (pH 8.5), 0.2 M LiCl, and 5–15% (w/v) polyethylene glycol (PEG) 4000.

Structure determination

X-ray diffraction data, including the single wavelength anomalous dispersion (SAD) data for the Se-Met-labeled crystals, were collected at Advanced Light Source (Berkeley, California, USA), Stanford Synchrotron Radiation Laboratory (Palo Alto, California, USA) and Advanced Photon Source (Argonne, Illinois, USA). All data were processed and reduced with Mosflm and scaled with Scala of the CCP4 suite of programs[40] using the software ELVES.[41] The space group of all crystals was determined to be $P6_5$, with the cell axes being 99 Å, 99 Å, 80 Å approximately and one protein monomer being present in the asymmetric unit. In co-crystals of Pim1 and small molecules, the cell and *b*-axes would occasionally double in size to accommodate four monomers in the asymmetric unit whenever minor conformational differences in monomers would perturb the crystal symmetry. The apo Pim1 structure was solved by SAD phasing with the Se-Met data at 2.6 Å resolution using the program SOLVE.[42] The electron density obtained after density modification by RESOLVE[42] was of sufficient quality to permit the building of the entire model using the program O.[43] This model was finally refined against a native dataset at 2.0 Å resolution using CNX (CNS[44] licensed to industrial users by Accelerys, Inc.) and refmac5.[45] All subsequent structures were determined by molecular replacement and refined by CNX and REFMAC5. The data processing and refinement statistics for a few key structures are shown in Table 1.

Kinase activity measurements

The *in vitro* kinase activities of wild-type and mutants were determined by measuring phosphorylation of biotinylated-BAD protein[6] using Perkin Elmer's AlphaScreen Technology. For each enzyme (0.01 ng), 20 μl reactions were carried out in 20 mM Hepes (pH 7.0), 10 mM $MgCl_2$, 1 mM DTT, 0.01% (v/v) Tween-20, 50 nM biotin-BAD protein and 1 mM ATP at room temperature. Reactions were stopped at five minutes with 5 μl of a solution containing 20 mM Hepes (pH 7.0), 200 mM NaCl, 80 mM EDTA, 0.3% (w/v) bovine serum albumin (BSA). The stop solution also included phospho-BAD (Ser112) antibody (Cell Signaling), streptavidin-coated donor beads and protein A acceptor beads. The antibody and beads were pre-incubated in stop solution in the dark at room temperature for 30 minutes. The final dilution of antibody was 1/2000 and the final concentration of each bead was 10 μg/ml. The assay plates were incubated at room temperature for one hour and then were read on a PerkinElmer AlphaQuest reader. Mutant activities are the average of two different batches of purified protein assayed in duplicate in three different experiments.

Coordinates

The coordinates and structure factors for the structures have been deposited with the RCSB Protein Data Bank (accession codes: 1YWV, 1YXS, 1YXT, 1YXU, 1YXX and 1YXV)

Table 1. Data processing and refinement statistics

	Pim1 Apo	Pim1 P123M	Pim1+AMPPNP	Pim1+AMP	Pim1+PLX-K031	Pim1+PLX-K063
A. Data processing						
Resolution (Å)	2.00	2.20	2.00	2.24	1.98	2.00
Unique refl.	30,439	23,005	28,438	84,753	29,825	29,461
R_{sym}[a,b]	0.048(0.719)	0.091(0.680)	0.057(0.715)	0.066(0.455)	0.057(0.369)	0.065(0.758)
Redundancy[b]	4.6(4.6)	4.3(4.3)	4.2(4.1)	4.1(4.1)	3.9(3.5)	4.0(3.5)
Completeness[b]	99.4(98.9)	99.8(100.0)	99.9(100.0)	97.3(96.7)	97.6(96.8)	99.7(99.2)
$\langle I/\sigma_I \rangle$[b]	14.3(1.8)	11.3(1.7)	14.0(1.5)	12.1(2.6)	16.5(1.7)	12.9(1.6)
B. Refinement						
Reflections used	30,224	22,949	28,380	82,479	29,111	27,964
R-factor[c]	0.211	0.195	0.181	0.228	0.218	0.188
R_{free}[d]	0.239	0.237	0.216	0.276	0.251	0.211
RMSD						
Bond lengths (Å)	0.012	0.011	0.013	0.013	0.012	0.009
Bond angles (deg.)	1.3	1.4	1.6	1.5	1.6	1.3

[a] $R_{sym} = \Sigma|I - \langle I \rangle| / \Sigma I$, where I is the intensity of a reflection and $\langle I \rangle$ is the mean intensity of multiple observations of that reflection as well as its symmetry mates.
[b] Values in parentheses refer to the highest resolution shell.
[c] R-factor $= \Sigma||F_o| - |F_c|| / \Sigma|F_o|$, where F_o and F_c are the observed and calculated structure factors of a given reflection, respectively.
[d] R_{free} was calculated by setting aside 5% of the reflections randomly.

Acknowledgements

We acknowledge Daniel Fong, Maryam Tabrizizad, Doug Yan, Brandi Grondona, Chris Bonagura, Heike Krupka, Graeme Card, Weiru Wang, and Kam Zhang for assistance in co-crystallization and crystallographic data collection. We thank Professor Axel Brunger for helpful discussions and advice with structure determination. Rafe Shellooe and Ben Powell expressed and purified large amounts of proteins for crystallography and assay. Jim Arnold and Yong-Liang Zhu participated in scaffold library construction and co-crystal structure analysis. We thank Professor Michael Lilly for the suggestion to use the BAD protein as substrate in the biochemical assay. Gaston Habets, Gideon Bollag and Professor Sung-Hou Kim offered numerous helpful suggestions and comments. We thank Peter Hirth and Mike Milburn for their generous advice and support.

References

1. Cuypers, H. T., Selten, G., Quint, W., Zijlstra, M., Maandag, E. R., Boelens, W. *et al*. (1984). Murine leukemia virus-induced T-cell lymphomagenesis: integration of proviruses in a distinct chromosomal region. *Cell*, **37**, 141–150.
2. van der Lugt, N. M., Domen, J., Verhoeven, E., Linders, K., van der Gulden, H., Allen, J. & Berns, A. (1995). Proviral tagging in E mu-myc transgenic mice lacking the Pim-1 proto-oncogene leads to compensatory activation of Pim-2. *EMBO J.* **14**, 2536–2544.
3. Feldman, J. D., Vician, L., Crispino, M., Tocco, G., Marcheselli, V. L., Bazan, N. G. *et al*. (1998). KID-1, a protein kinase induced by depolarization in brain. *J. Biol. Chem.* **273**, 16535–16543.
4. Winn, L. M., Lei, W. & Ness, S. A. (2003). Pim-1 phosphorylates the DNA binding domain of c-Myb. *Cell Cycle*, **2**, 258–262.
5. Yan, B., Zemskova, M., Holder, S., Chin, V., Kraft, A., Koskinen, P. J. & Lilly, M. (2003). The PIM-2 kinase phosphorylates BAD on serine 112 and reverses BAD-induced cell death. *J. Biol. Chem.* **278**, 45358–45367.
6. Aho, T. L., Sandholm, J., Peltola, K. J., Mankonen, H. P., Lilly, M. & Koskinen, P. J. (2004). Pim-1 kinase promotes inactivation of the pro-apoptotic Bad protein by phosphorylating it on the Ser112 gatekeeper site. *FEBS Letters*, **571**, 43–49.
7. Chen, X. P., Losman, J. A., Cowan, S., Donahue, E., Fay, S., Vuong, B. Q. *et al*. (2002). Pim serine/threonine kinases regulate the stability of Socs-1 protein. *Proc. Natl Acad. Sci. USA*, **99**, 2175–2180.
8. Mochizuki, T., Kitanaka, C., Noguchi, K., Muramatsu, T., Asai, A. & Kuchino, Y. (1999). Physical and functional interactions between Pim-1 kinase and Cdc25A phosphatase. Implications for the Pim-1-mediated activation of the c-Myc signaling pathway. *J. Biol. Chem.* **274**, 18659–18666.
9. Koike, N., Maita, H., Taira, T., Ariga, H. & Iguchi-Ariga, S. M. (2000). Identification of heterochromatin protein 1 (HP1) as a phosphorylation target by Pim-1 kinase and the effect of phosphorylation on the transcriptional repression function of HP1(1). *FEBS Letters*, **467**, 17–21.
10. Maita, H., Harada, Y., Nagakubo, D., Kitaura, H., Ikeda, M., Tamai, K. *et al*. (2000). PAP-1, a novel target protein of phosphorylation by pim-1 kinase. *Eur. J. Biochem.* **267**, 5168–5178.
11. Wang, Z., Bhattacharya, N., Mixter, P. F., Wei, W., Sedivy, J. & Magnuson, N. S. (2002). Phosphorylation of the cell cycle inhibitor p21Cip1/WAF1 by Pim-1 kinase. *Biochim. Biophys. Acta*, **1593**, 45–55.
12. Wang, Z., Bhattacharya, N., Meyer, M. K., Seimiya, H., Tsuruo, T., Tonani, J. A. & Magnuson, N. S. (2001). Pim-1 negatively regulates the activity of PTP-U2S phosphatase and influences terminal differentiation and apoptosis of monoblastoid leukemia cells. *Arch. Biochem. Biophys.* **390**, 9–18.
13. Rainio, E. M., Sandholm, J. & Koskinen, P. J. (2002). Cutting edge: transcriptional activity of NFATc1 is enhanced by the Pim-1 kinase. *J. Immunol.* **168**, 1524–1527.
14. Wang, Z., Bhattacharya, N., Weaver, M., Petersen, K., Meyer, M., Gapter, L. & Magnuson, N. S. (2001). Pim-1: a serine/threonine kinase with a role in cell survival, proliferation, differentiation and tumorigenesis. *J. Vet. Sci.* **2**, 167–179.
15. Mikkers, H., Nawijn, M., Allen, J., Brouwers, C., Verhoeven, E., Jonkers, J. & Berns, A. (2004). Mice deficient for all PIM kinases display reduced body size and impaired responses to hematopoietic growth factors. *Mol. Cell. Biol.* **24**, 6104–6115.
16. Lilly, M. & Kraft, A. (1997). Enforced expression of the Mr 33,000 Pim-1 kinase enhances factor-independent survival and inhibits apoptosis in murine myeloid cells. *Cancer Res.* **57**, 5348–5355.
17. Lilly, M., Sandholm, J., Cooper, J. J., Koskinen, P. J. & Kraft, A. (1999). The PIM-1 serine kinase prolongs survival and inhibits apoptosis-related mitochondrial dysfunction in part through a bcl-2-dependent pathway. *Oncogene*, **18**, 4022–4031.
18. Moroy, T., Grzeschiczek, A., Petzold, S. & Hartmann, K. U. (1993). Expression of a Pim-1 transgene accelerates lymphoproliferation and inhibits apoptosis in lpr/lpr mice. *Proc. Natl Acad. Sci. USA*, **90**, 10734–10738.
19. Lilly, M., Le, T., Holland, P. & Hendrickson, S. L. (1992). Sustained expression of the pim-1 kinase is specifically induced in myeloid cells by cytokines whose receptors are structurally related. *Oncogene*, **7**, 727–732.
20. Amson, R., Sigaux, F., Przedborski, S., Flandrin, G., Givol, D. & Telerman, A. (1989). The human proto-oncogene product p33pim is expressed during fetal hematopoiesis and in diverse leukemias. *Proc. Natl Acad. Sci. USA*, **86**, 8857–8861.
21. Dhanasekaran, S. M., Barrette, T. R., Ghosh, D., Shah, R., Varambally, S., Kurachi, K. *et al*. (2001). Delineation of prognostic biomarkers in prostate cancer. *Nature*, **412**, 822–826.
22. Ellwood-Yen, K., Graeber, T. G., Wongvipat, J., Iruela-Arispe, M. L., Zhang, J., Matusik, R. *et al*. (2003). Myc-driven murine prostate cancer shares molecular features with human prostate tumors. *Cancer Cell*, **4**, 223–238.
23. Kim, O., Jiang, T., Xie, Y., Guo, Z., Chen, H. & Qiu, Y. (2004). Synergism of cytoplasmic kinases in IL6-induced ligand-independent activation of androgen receptor in prostate cancer cells. *Oncogene*, **23**, 1838–1844.
24. Akasaka, H., Akasaka, T., Kurata, M., Ueda, C., Shimizu, A., Uchiyama, T. & Ohno, H. (2000).

Molecular anatomy of BCL6 translocations revealed by long-distance polymerase chain reaction-based assays. *Cancer Res.* **60**, 2335–2341.
25. Pasqualucci, L., Neumeister, P., Goossens, T., Nanjangud, G., Chaganti, R. S., Kuppers, R. & Dalla-Favera, R. (2001). Hypermutation of multiple proto-oncogenes in B-cell diffuse large-cell lymphomas. *Nature*, **412**, 341–346.
26. Montesinos-Rongen, M., Van Roost, D., Schaller, C., Wiestler, O. D. & Deckert, M. (2004). Primary diffuse large B-cell lymphomas of the central nervous system are targeted by aberrant somatic hypermutation. *Blood*, **103**, 1869–1875.
27. Gaidano, G., Pasqualucci, L., Capello, D., Berra, E., Deambrogi, C., Rossi, D. *et al*. (2003). Aberrant somatic hypermutation in multiple subtypes of AIDS-associated non-Hodgkin lymphoma. *Blood*, **102**, 1833–1841.
28. Qian, K. C., Wang, L., Hickey, E. R., Studts, J., Barringer, K., Peng, C. *et al*. (2004). Structural basis of constitutive activity and a unique nucleotide binding mode of human Pim-1 kinase. *J. Biol. Chem.* **280**, 6130–6137.
29. Card, G. L., Blasdell, L., England, B. P., Zhang, C., Suzuki, Y., Gillette, S. *et al*. (2004). A new family of phosphodiesterase inhibitors discovered by co-crystallography and scaffold-based drug design. *Nature Biotechnol*. In the press.
30. Selten, G., Cuypers, H. T., Boelens, W., Robanus-Maandag, E., Verbeek, J., Domen, J. *et al*. (1986). The primary structure of the putative oncogene pim-1 shows extensive homology with protein kinases. *Cell*, **46**, 603–611.
31. Taylor, S. S. & Radzio-Andzelm, E. (1994). Three protein kinase structures define a common motif. *Structure*, **2**, 345–355.
32. Knighton, D. R., Zheng, J. H., Ten Eyck, L. F., Ashford, V. A., Xuong, N. H., Taylor, S. S. & Sowadski, J. M. (1991). Crystal structure of the catalytic subunit of cyclic adenosine monophosphate-dependent protein kinase. *Science*, **253**, 407–414.
33. Johnson, L. N., Noble, M. E. & Owen, D. J. (1996). Active and inactive protein kinases: structural basis for regulation. *Cell*, **85**, 149–158.
34. Hardcastle, I. R., Golding, B. T. & Griffin, R. J. (2002). Designing inhibitors of cyclin-dependent kinases. *Annu. Rev. Pharmacol. Toxicol.* **42**, 325–348.
35. Mohammadi, M., McMahon, G., Sun, L., Tang, C., Hirth, P., Yeh, B. K. *et al*. (1997). Structures of the tyrosine kinase domain of fibroblast growth factor receptor in complex with inhibitors. *Science*, **276**, 955–960.
36. Davis, S. T., Benson, B. G., Bramson, H. N., Chapman, D. E., Dickerson, S. H., Dold, K. M. *et al*. (2001). Prevention of chemotherapy-induced alopecia in rats by CDK inhibitors. *Science*, **291**, 134–137.
37. Manning, G., Whyte, D. B., Martinez, R., Hunter, T. & Sudarsanam, S. (2002). The protein kinase complement of the human genome. *Science*, **298**, 1912–1934.
38. Wan, P. T., Garnett, M. J., Roe, S. M., Lee, S., Niculescu-Duvaz, D., Good, V. M. *et al*. (2004). Mechanism of activation of the RAF-ERK signaling pathway by oncogenic mutations of B-RAF. *Cell*, **116**, 855–867.
39. Hendrickson, W. A., Horton, J. R. & LeMaster, D. M. (1990). Seleno-methionyl proteins produced for analysis by multiwavelength anomalous diffraction (MAD): a vehicle for direct determination of three-dimensional structure. *EMBO J.* **9**, 1665–1672.
40. Collaborative Computational Project Number 4. (1994). The CCP4 suite: programs for protein crystallography. *Acta Crystallog. sect. D*, **50**, 760–763.
41. Holton, J. & Alber, T. (2004). Automated protein crystal structure determination using ELVES. *Proc. Natl Acad. Sci. USA*, **101**, 1537–1542.
42. Terwilliger, T. C. (2003). SOLVE and RESOLVE: automated structure solution and density modification. *Methods Enzymol.* **374**, 22–37.
43. Jones, T. A., Zou, J. Y., Cowan, S. W. & Kjeldgaard (1991). Improved methods for building protein models in electron density maps and the location of errors in these models. *Acta Crystallog. sect. A*, **47**, 110–119.
44. Brunger, A. T., Adams, P. D., Clore, G. M., DeLano, W. L., Gros, P., Grosse-Kunstleve, R. W. *et al*. (1998). Crystallography & NMR system: a new software suite for macromolecular structure determination. *Acta Crystallog. sect. D*, **54**, 905–921.
45. Winn, M. D., Isupov, M. N. & Murshudov, G. N. (2001). Use of TLS parameters to model anisotropic displacements in macromolecular refinement. *Acta. Crystallog. sect. D*, **57**, 122–133.
46. DeLano, W. L. (2004). *The PyMOL Molecular Graphics System*, 0.95 edit. DeLano Scientific LLC, San Carlos, CA, USA.

Edited by I. Wilson

(Received 13 December 2004; received in revised form 17 February 2005; accepted 18 February 2005)